https://doi.org/10.1016/j.ssc.2016.03.010

Strong compensation hinders the p-type doping of ZnO : a glance over surface defect levels

B. Huang*

Department of Applied Biology and Chemical Technology, The Hong Kong Polytechnic University, Hung Hom, Kowloon, Hong Kong SAR, China

*Email: bhuang@polyu.edu.hk

Abstract

The defect compensation as dominant source restricts the Fermi level in ZnO to approach an easy p-type before to be the heavy degenerated doping object. We discussed the surface defect levels to elucidate this nature. The defect states on the dominant growth surface (0001) show a stronger compensating effect compared to the bulk state. Both substitution and adatom nitrogen doping shows it provides an extremely deep donor and acceptor lead to an unchanged Fermi level within the band gap but to be pinned in the mid-gap by bulk doping. As the dimension of the ZnO materials further decreases to be monolayer, the quantum confinement effect even more localized and render the charge transfer on surface to restrict the shifting of Fermi level. We report this can overwhelm the intrinsic p-type conductivity and transport of the ZnO bulk system, and further pinned the Fermi level in the monolayer ZnO and graphene interface system.

Introduction

ZnO materials as II-VI semiconductor compounds have a large direct band gap of 3.4 eV[1]. They are accordingly prime candidates for blue and ultraviolet light-emitting diodes and lasers. However, the fabrication of the p-n junction for light-emitting diodes is very difficult [2, 3]. Like most wurtzite II-VI compounds, they have intrinsic n-type conductivities, while the p-type doping is not yet well developed. All the research related to p-type doping indicates that this is due to the "self-compensation" of shallow acceptors by various natively occurring or spontaneously generated donor defects, such as vacancies or interstitials. However, as expected, the shallow acceptor candidate elements have been shown to provide deep levels in the gap as trapping centers of the host ZnO lattice. This arises because the anticipated shallow group-V acceptors in ZnO have higher thermal ionization energy barriers (or, in other words, transition energies of different charge states), causing them to yield at a deep level near the midgap [4].

We are inspired by surface quantum confinement effect of ZnO nanomaterials studied by Dalpian et al[5, 6]. The ZnO nanomaterials such as nanowires or nanodots with controllable size and morphologies are seen as having potential for the next generation of the electronics industry. The surface becomes more dominant as the quantum confinement becomes more evident with the increasing surface-to-volume ratio[7, 8]. Therefore, it is important to unravel the technological difficulties of achieving p-type doping in view of the possible applications of ZnO nanomaterials.

Among those group-V candidates, N is the best choice as it has similar atomic radius and electronegativity to O. Experimentally, the N in ZnO nanomaterials has been reported to modify the conductivity of the p-type. However, the high cost of doing so may hinder the pace of development. N is not very soluble in these II-VI wide band gap semiconductor materials, and doping with N in bulk may be achievable only by ion implantation. However, N-acceptor dopant is still a possibility given that it was verified by luminescence measurements on N^+-implanted ZnSe as early as 1982, in the work of Wu et al. [9]. On the other hand, our previous study on group VI based chalcogenide shows the N doping will increase the local structural distortion, and provide localized edge states in order to enhance the band-overlapping lead to pinning of Fermi level (E_F)[10, 11]. Meanwhile, the defect level study has proved to be a useful concept to understand the electrical conductions and transport mechanism[11, 12].

Theoretically, the N doping level in the electronic structure of ZnO is unclear. It has been reported to sit relatively deep in the gap and also to contain errors of band structure calculations, as shown in the local density approximation (LDA) calculations of Park et al. [13] and Li et al [14]. More accurate results obtained by hybrid functionals shows that the N-substitutional doping on the O site is in fact a deep acceptor with a high thermal ionization energy of 1.3 eV to vary the charge state (accepting electrons) [15]. However, this still does not explain why N cannot be a good candidate. Moreover, the p-type doping of low-dimensional ZnO nanomaterials has been achieved experimentally. This discrepancy may be due to the lack of information about the native defects environments of ZnO, which has many native point defects contributing to the intrinsic n-type conductivity. Also, the dimensional difference shows a large contrast in the electronic properties of nanomaterials, since the large surface-to-volume ratio causes the surface quantum confinement to be more dominant in materials. Drawing on this previous work, we recognize that the native point defects forming on the surface of ZnO can modify their electronic

conductivities. Therefore, we suggest possible ways to achieve better p-type ZnO with N-dopant to overcome the effect of bulk intrinsic defects.

Experimental section

Our first-principles calculations are based on the generalized gradient approximation (GGA)+U method with rotational invariant U parameter on localized orbitals[16, 17], which is the simplest way to reflect the contrast in the electronic properties of the surface and bulk based on the correct reproduction of the band structure calculations for the bulk. Such method has been successfully applied in many solid functional materials (oxides and sulfides) by us, for discussions on their electronic structures and defect levels as well as its formation energies [18-20]. To model the ZnO(0001) surface system, we built a periodic slab structure containing four Zn-O bilayers with a vacuum layer of more than 15 Å for separation. We used a 4×4 ZnO unit cell to model the two-dimensional surface. In order to accurately reflect the stabilization mechanism of the Zn-terminated surface, the model we built had to be terminated with a 0.5 monolayer of H on the unreconstructed O-terminated back surface, which serves as a hydroxyl group to stabilize the system induced by the spurious charge proposed by Meyer [21].

The Anisimov-type rotation invariant Hubbard-U correction on the fully filled 3d orbitals of the Zn atoms are chosen to be 10 eV [17, 22], and the U parameter for correcting the $3d^{10}$ orbital level is self-consistently determined by using our previous method[23]. The Hubbard-U correction on 2p orbitals of O atoms follows the work of Ma et al[24]. To reduce the influence of the valence-core charge density overlapping, we used the nonlinear core correction method to reconstruct the Zn pseudopotential based on the Kleimann-Bylander norm-conserving type. In the overall calculation, we set the plane wave basis set for the kinetic energy expansion as 750 eV, which is enough for metal oxides. The Monkhorst-Pack k-point grid for the ZnO (0001) surface system calculations was chosen as 2×2×1. For the related defect state geometry relaxation, the geometric optimization used the Broyden-Fletcher-Goldfarb-Shannon (BFGS) algorithm for all bulk and defect supercell calculations.

For the calculation of the defect formation energy in different charge states, the overall supercell size was fixed based on the relaxed neutral bulk unit cell. The defect formation energy (H_q) at the charge state q as a function of the Fermi energy (E_F) and the chemical potential $\Delta\mu$ of element α is given by

$$H_q(E_F,\mu) = E_q - E_H + q\left(E_V + \Delta E_F\right) + \sum_\alpha n_\alpha\left(\mu_\alpha^0 + \Delta\mu_\alpha\right), \quad (1)$$

where E_q and E_H are the total energy of a defect and perfect cell, respectively, calculated with charge q; ΔE_F is the Fermi energy with respect to the valence band maximum; n_α is the number of atoms of element α; and μ_α^0 is the reference chemical potential, following Lany and Zunger [25]. To calibrate our calculation settings, we carried out a pretest on the bulk ZnO model. The band gap of the bulk model obtained was 3.44 eV (error: 1.2%) with lattice parameters of 3.248 and 5.216 Å, respectively. Considering the differences between the bulk and native point defect calculations, we further tested for the O vacancy (V_O) under the O-poor chemical potential limit, and obtained a formation energy of V_O as 0.963 eV. This is reasonably consistent with the results

of Oba et al. (0.96 eV, and 1.01 eV) using HSE in VASP [26] and Robertson et al. (0.85 eV) using sX-LDA in CASTEP, respectively [27-29].

Results and discussion

Transition levels

The present work performed a calculation on the N-adatom (A_N) surface doping. The N atom has a similar atomic radius to O (0.75 Å vs 0.73 Å). Its p-orbital has a half-filled configuration ($2p^3$) that can either accept or donate electrons depending on the growth environment. Therefore, we performed the A_N doping calculations within seven charge states (-3, -2, -1, 0, 1, 2, and 3).

We found that the N-substituting doping on the O-site (N_O), which is a widely accepted theoretical model for promising acceptors, gives a high p-type conductivity for ZnO[30-32]. However, there will be many contradictions if we simply attribute the p-type conduction with the experimentally observed 100~200 meV hole ionization energy to the N_O doping [32-34]. Moreover, Lany and Zunger discussed how the assumed shallow acceptor states of N are difficult to reconcile with the strongly localized Jahn-Teller distortion induced by localized hole states from the 2p orbitals [35, 36]. The issue is which of these effects contributes the shallow acceptor levels (less than 0.2 eV) observed from experiment. Lany and Zunger use both the generalized Koopman theory and hybrid functional (HSE) to predict a deep ionization energy for the N_O:ZnO of 1.62 eV, which confirms the deep-level behavior of N_O in the bulk [35, 36]. Recently, Liu et al. have shown that the N_{Zn}-V_O complex in ZnO could play an important role in giving a shallow state [37]. However, this lacks the correct band gap predicted by the hybrid functional, so the question is why the formation enthalpy of ZnO has a +0.2 eV error compared to the experimental figure of -3.61 eV/ZnO [38]. Meanwhile, the N_{Zn} imposes a large energy cost (about 5.6 eV) in ZnO, which makes it difficult for it to form in the lattice [37]. However, this surface model is remarkable, even though a better understanding of the effect of surface states is still required.

Accordingly, we show our theoretical model in Fig. 1. The defects or impurities on the ZnO(0001) polar surface may lead to rater deeper acceptor or donor states (Fig. 1), since the bulk central potential is screened by the surface polar charge accumulation layer [39, 40], propelling the surface defect states to fall into the deep levels by surface Coulomb potential effect (Fig. 1). We propose that due to the large polarity and strong surface quantum confinement for electrons, the conventional bulk doping technology should be modified to a surface passivation doping, which leads to a large and effective charge transfer, in order to meet the p/n-type doping requirements of industry. It is more efficient to observe the charge transition level in the band gap, which denotes the defect or dopants thermal ionization energy. For different charge state q and q', the critical level that changes with related to Fermi level in the band gap is the transition level, $\varepsilon(q/q')$. As calculated by DFT procedure in terms of following equation.

$$\varepsilon(q/q') = \frac{E_f(D^q) - E_f(D^{q'})}{q' - q} \qquad (2)$$

Where the $E_f(D^q)$ is the formation energy of the defect or dopant in the charge state of q. $E_f(D^{q'})$ is the formation energy of the same defect or dopant stabilize in the charge state of q'. The details form has been similar discussed by Janotti et al[38]. It is advantageous to use the idea

of transition level because it can be observed in experiments where the final charge state of the local structure is capable to fully relax towards its equilibrium state after the charge transition or thermal ionization, by deep-level transient spectroscopy (DLTS)[41].

Surface native point defect levels and nitrogen doping

Fig. 2 (a) and (b) summarize the native point defect levels on the (0001) surface of ZnO. We see that all of the defects are negative-U defects, which cannot be evidently detected by the electron spin resonance (ESR) measurements. Such defect levels on the surface are actually playing as "dopant-killer" for ZnO related nanomaterials. This arises because the previous found deep donor-trap defects like V_O and I_{Zn} in the bulk ZnO now turn to be the rather deeper defects close the band edges on the surface. The trend is the same as the acceptor-trap defects like V_{Zn} and I_O. Fig. 2 (c) shows our results of formation energy against Fermi energy of N-substitution in the bulk ZnO and N surface passivation doping on the ZnO(0001) surface. It can be seen that the N_O in the bulk ZnO is not only a deep-level impurity within the band gap, but also gives an E_F pinning deep in the midgap at about 1.57 eV. This arises because the critical position of $\varepsilon(-/+)$ in E_F has the lowest energy even lower than the neutral state of the N-dopant, which is the dip of the red solid curve of the Fig. 2(c). This is very close to the prediction of Lany and Zunger using the generalized Koopmans theory. However, we show more details, with the E_F pinning effect used to confirm that the N substitution in the bulk induces low conductivity of the host ZnO. We take the neutral N_O in the ZnO formation energy as our zero energy reference; accordingly, the surface N-adatom (surface A_N) and N-substitution (surface N_O) have even lower energies compared to the formation in the bulk. This may be due to the large surface interaction of the low-dimensional ZnO. Moreover, it can be seen from Fig. 2 (c) and (d) that the surface N_O performs poorly as a surface compensation dopants due to a shallow acceptor (0.72 eV) as gap states to trap the E_F. In fact, it is deeper than the case of the surface A_N (0.14 eV) in the hole ionization energy from the charge -3 to 0 states. We also show that thermal ionization occurs from -3 or -2 to 0 and then to +3, resulting in a negative effective correlation energy (negative-U_{eff}). The result of our surface A_N is close to the experimental observation, and also contributes to the near-delocalized states next to the valence band edge.

From Fig. 3 (a), it can be seen that the N-dopants on ZnO(0001) show a clear contrast in the local structure relaxations between the +3 and 0 or -3 states. Note also that the N^{3+} dopant as adatom (A_N^{3+}) has the lowest formation energy level, compared to the A_N^0 and A_N^{3-} states. Moreover, the A_N^{3+} has an orientation towards the preferred charge localization on the surface of the ZnO(0001) with a loss of three-fold symmetry. The tri-positively charged configuration leads the valence electrons of N to have π-like $2s^2$ lone-pair electrons weakly interacting with the neighboring unsaturated Zn atom. From Fig. 3 (b), it can be seen that A_N^{3+} makes a passive contribution to the local electronic density of the states of ZnO(0001) and is only a shallow state at about 1.6 eV above the charge-neutral line (0 eV). Note also that the charge-neutral line is totally different from the case of bulk ZnO. These localized states are evidently different to the case of the bulk as shown in Fig. 4, and the localized hole state shown in Fig. 4 has a similar p_z orbital feature as that shown by Lany and Zunger [23].

Experimentally, N-doping is performed using the method of N_2O gaseous doping, which means the chemical potential of the N needs to reach the N-rich limit [42]. Such an experiment

raises issues about stability at the ambient temperature [43]. However, the O gaseous atmosphere in ambient conditions means the ZnO nanomaterials deform the N-doping layer. Our calculations show that an investigation of formation energy can explain this scenario. In Fig. 3(a), N-doping in the neutral state matches our deduced doping limit range given by the native defects of ZnO(0001), and the A_N^0 may even remain lower than the A_O under the N-poor condition. The N_2O gas phase means the sample is N-rich, pushing up the formation energy even higher than the V_{Zn} under the N-rich condition that shows up as being O-rich. The difficulty in the doping process then becomes focused on the subtle equilibriums of the N and O chemical potentials during the doping growth process.

Monolayer ZnO interface with graphene system

As is well known, ZnO is a wide band gap semiconductor oxide with direct gap of about 3.4 eV (in 300K), and its monolayer can be used as charge trapping layer in CMOS memory cell. Recent study shows that the monolayer ZnO can be interfaced with graphene acting as a good substrate for topological insulator (TI), since the dirac-cone retains and is pinned near the midgap of the monolayer ZnO, regardless the existence of the intrinsic defects[44-47]. Meanwhile, the interface charge transfer between monolayer ZnO and graphene layer are a promising area of 2-D electronic modulation as applications of high-speed electronic response devices. As shown in the comparison from the Figure 5 (a) and (b), we found the band structure and density of states occur tail states due to the long range crystal field interaction missing vertically to ZnO(0001), and the 3d levels have been split into two peaks due to a evident contrast of p-d coupling along and perpendicular to ZnO(0001). The band gap has widen to 3.57 eV compared to 3.41 eV in bulk phase from our calculations. The starting point of 3d level is 0.5 eV deeper than the one in the bulk (-7.0 eV we got in calculation.). The formation entropy of the bulk ZnO is -3.70 eV which is consistent to the experimentally reported -3.60 eV in 300K. Figure 5 (a) and (b) give the basic electronic properties of bulk wurtzite and monolayer of ZnO, respectively.

The oxygen hole states levels have been long interested in the metal oxides or wide band gap semiconductors, particularly in the ZnO[35, 48], the localized hole levels move the Fermi level towards deep in the gap. We investigate the single zinc vacancy (V_{Zn}) as it can induce two holes localized around nearby O-sites. However, this cannot clearly given by LDA/GGA calculations as the homogenous electron gas treats the two hole states degenerated into one and delocalized around the V_{Zn} site. Our GGA+U calculation with stabilizing the hole states can give clear electron-hole interaction under different charge states, as shown in Figure 5 (c). This has been also reported by our previous work[18]. Figure 5 (d) shows the neutral V_{Zn} has negative effective correlation U (negative-U_{eff}) of -0.57 eV, for the process of $2(V_{Zn}^0) \rightarrow (V_{Zn}^+) + (V_{Zn}^-)$. Such exothermal reaction means one of the O-site acting as acceptors capturing two electrons easily overcoming the onsite Coulomb repulsive energy, which are the nearest neighbor of V_{Zn}^0. The other two localized hole states turns to be repulsive to each other while the electron acceptor sites that move towards to the hole sites. This shows a planar Jahn-Teller distortion effect that the symmetry lowers from D_{3h} down to the D_{2h}. The other two charge states, V_{Zn}^+ and V_{Zn}^-, also have the same trends. The total energy of the system lowers with structural relaxation. From Figure 5 (e), we also found that the localized hole states have the π-like orbital next to the conduction band minimum, and perpendicular to the plane (0001) in real space with p_z-orbital character (with a_1-symmetry). However, the electron acceptor site has similar π-like orbital along

the (0001) plane, which is a feature of p_{xy}-orbital. This interesting behavior leads the monolayer ZnO system has an anti-ferromagnetic feature with existence of single neutral V_{Zn}.

We can also find that the hole and electron levels are not free-charge-carrier supplying center as they are localized as trap states. The intrinsic conductivity of the monolayer ZnO may largely restricted by such native defects. The E_F was actually pinned near the midgap. If we extend the system to interface with graphene layer, the position of dirac-cone (cone level) will be pinned near the midgap of the ZnO owing to the subtle electron-holes interactions (illustrated in Figure 5 (f)). The reason that the Jahn-Teller distortion occurs in the monolayer ZnO with V_{Zn} is because the asymmetry between the occupancies of $p_{x,y}$ and p_z orbitals within the planar monolayer ZnO is getting larger than the non-centrosymmetrical bulk wurtzite ZnO. This asymmetry can be also found in ZnO but negligible[48].

Conclusion

In summary, we show that in transparent semiconducting oxides such as ZnO, the native defect states that act as native surface passivants on the ZnO surface play a key role in modifying the electronic transport and conductivity of the host system. The related surface states can mask the effect of the dopants or native point defects from the bulk system. The neutral N-stabilized material is a good match for the doping limit range provided by the native defects of the ZnO(0001) surface. The tri-positively charged N on the ZnO(0001) surface an extremely deep donor and acceptor lead to an unchanged Fermi level within the band gap but to be pinned in the mid-gap by bulk doping, meanwhile the specifically oriented charge localization may also change the low-dimensional growth direction of the ZnO after N-doping. This is close to previous experimental findings. As the dimension of the ZnO materials further decreases to be monolayer, the quantum confinement effect even more localized and render the charge transfer on surface to restrict the shifting of Fermi level. We propose that the surface defect states or extrinsic dopants effects overwhelm the intrinsic p-type conductivity and transport of the ZnO bulk system. This leads to an interesting and practically difficult problem.

Acknowledgement

The author gratefully acknowledges the support of the Natural Science Foundation of China (NSFC) for the Youth Scientist grant (Grant No. NSFC 11504309) and the initial start-up grant support from the Department General Research Fund (Dept. GRF) from ABCT in the Hong Kong Polytechnic University.

Fig. 1

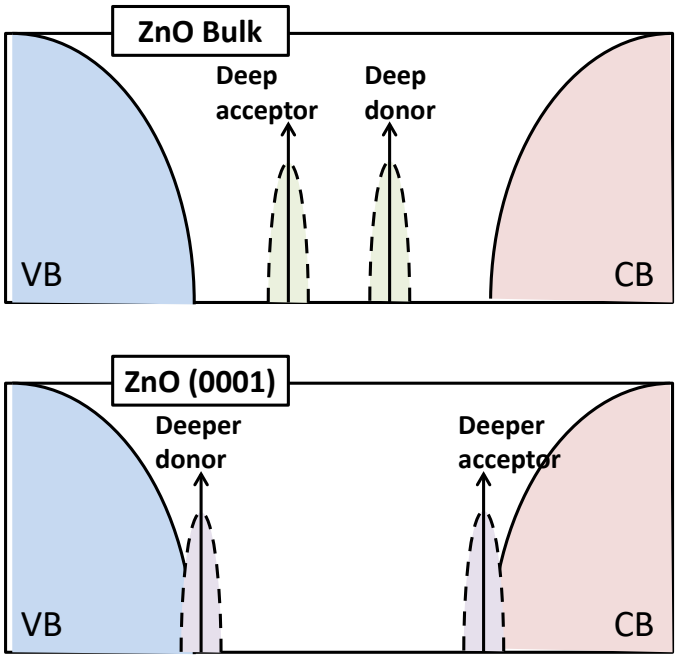

Fig. 1 Schematic diagram of the role of native point defects as a surfactant that modifies the conduction.

Fig. 2

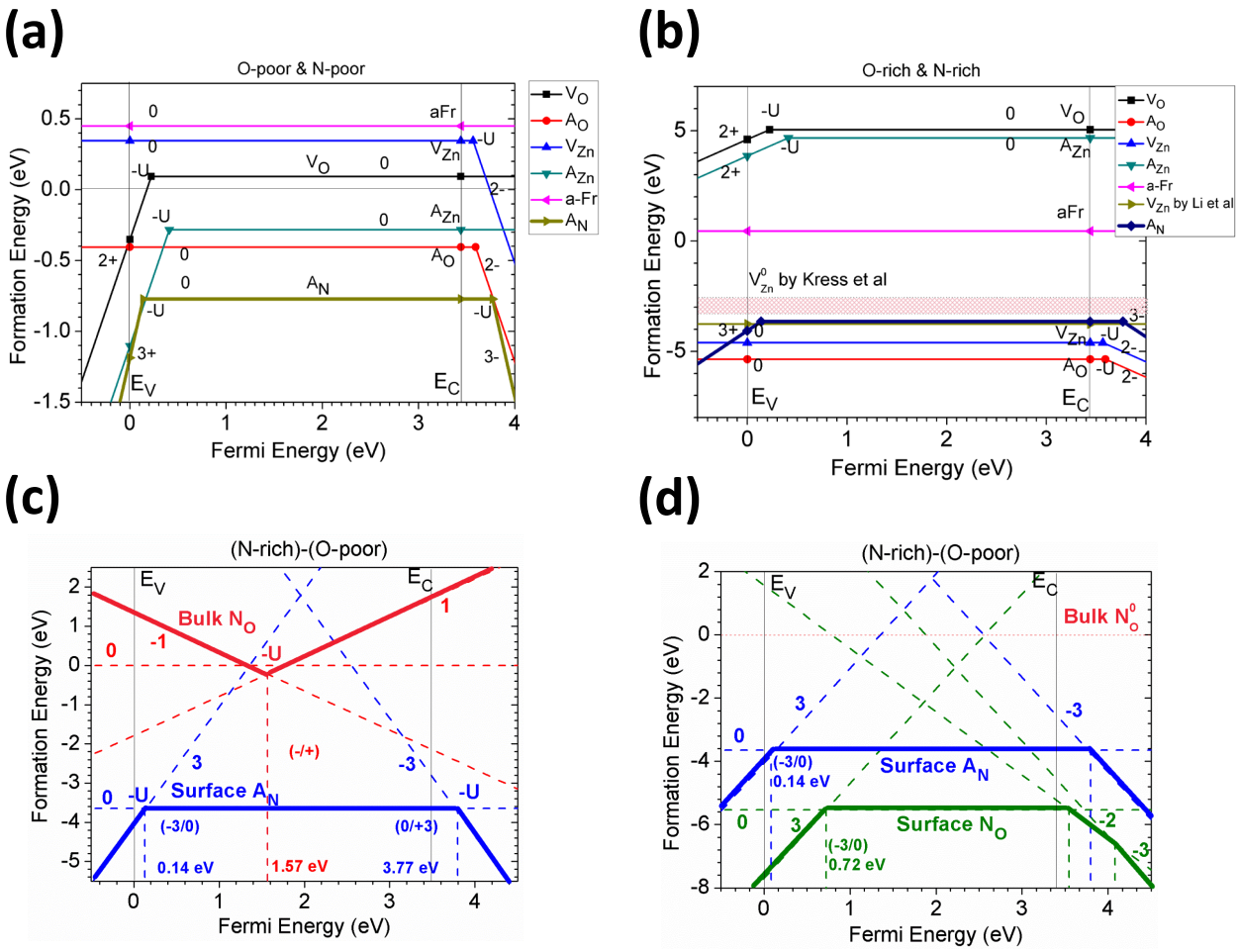

Fig. 2 Formation vs Fermi energy of surface native defects levels (a) and (b); the N-adatom (A_N) and N-substitution (N_O) in the bulk ZnO and N surface doping on the ZnO(0001) surface (c) and (d).

Fig. 3

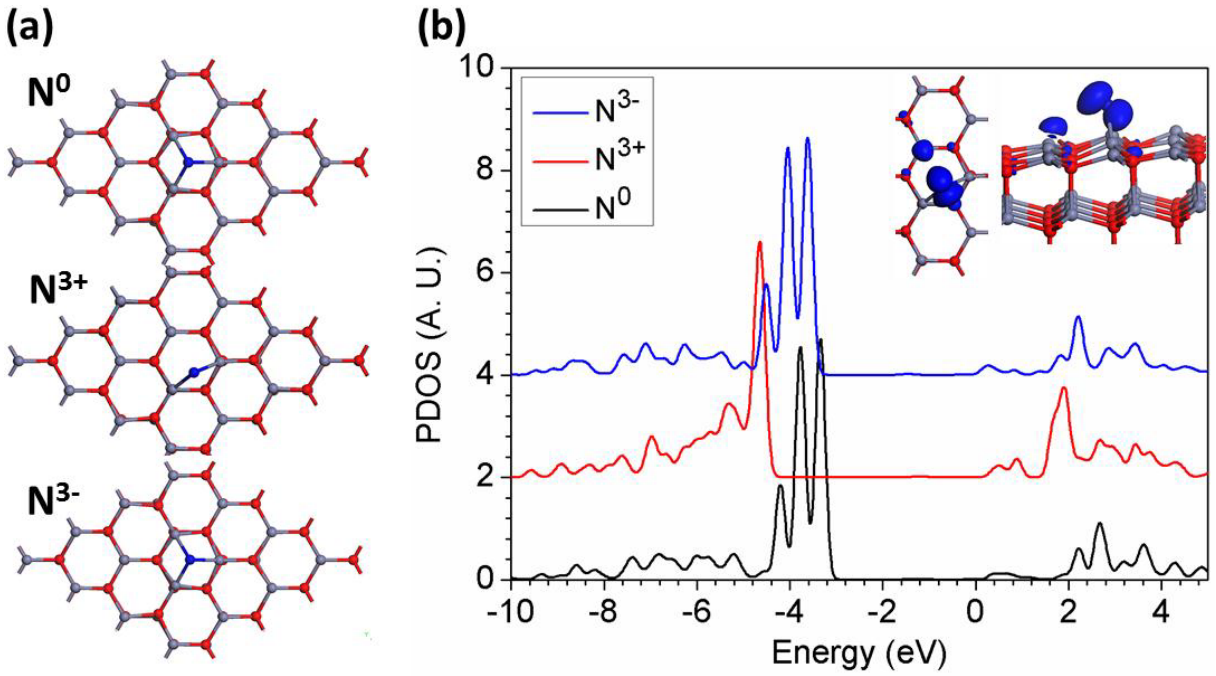

Fig. 3. (a) Local relaxed structures of N passivation doping in three different charge states (0, +3, and -3). (b) Partial density of states (PDOS) of N on the ZnO(0001) surface. The upper right inset figures are the top and side views of the contours of the N local charge states.

Fig. 4

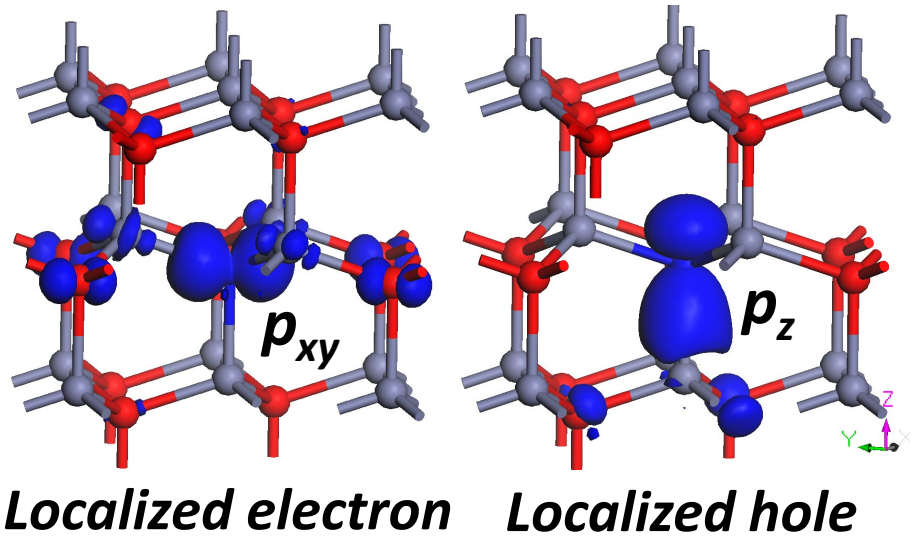

Fig. 4 The localized electron (left) and hole (right) states induced by N_O in bulk ZnO, with p_{xy} and p_z orbital features, respectively.

Figure 5

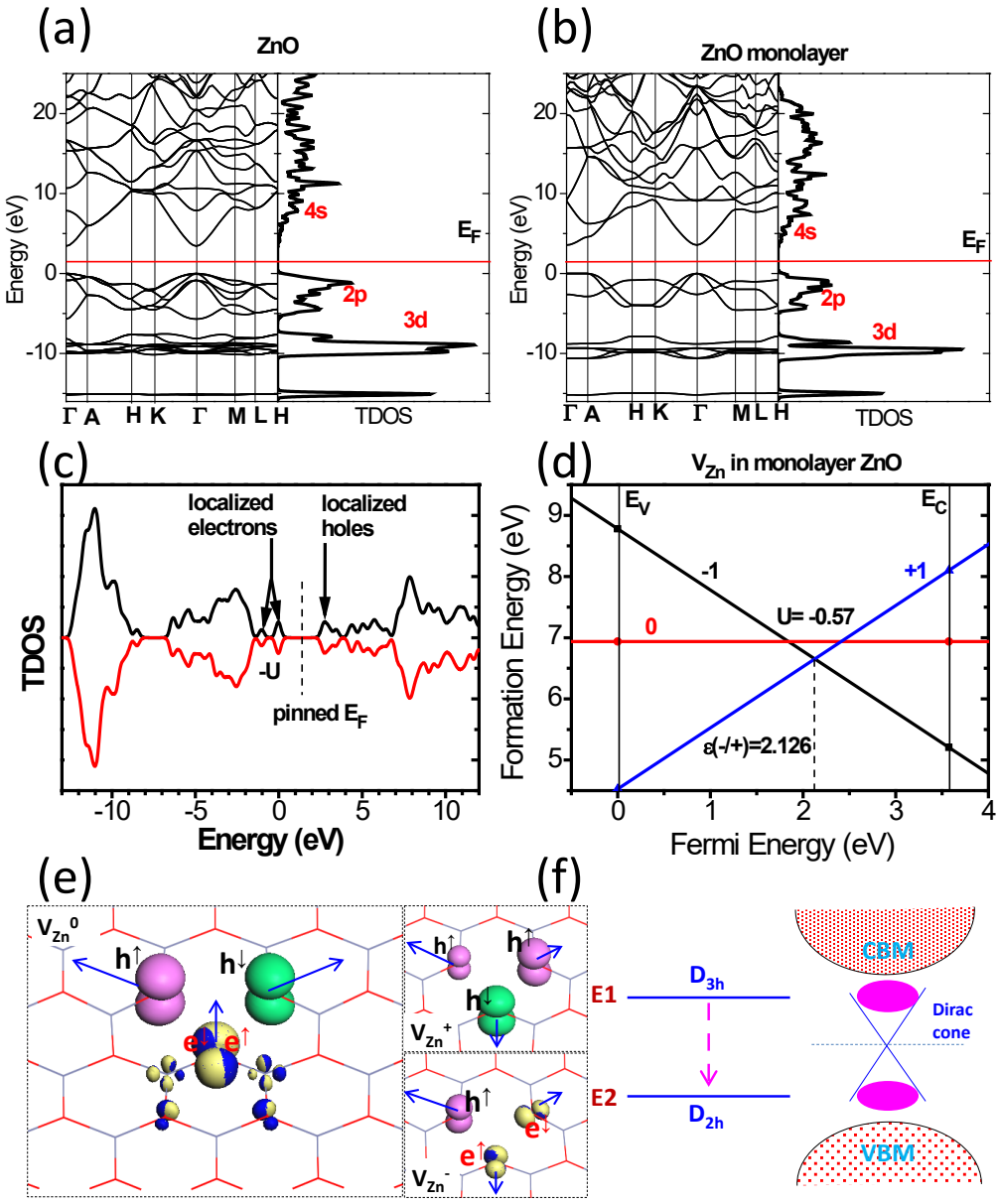

Figure 5. (a) Electronic band structure and total density of states (TDOS) of wurtzite ZnO with estimated band gap of 3.407 eV. (b) Electronic band structure and total density of states (TDOS) of planar monolayer ZnO with estimated band gap of 3.573 eV. (c) TDOS of monolayer ZnO system with intrinsic neutral Zn vacancy (V_{Zn}^0). (d) Formation energy vs Fermi energy within different charge states of -1, 0, and +1, for V_{Zn} in monolayer of ZnO. (e) Localized orbitals electron and oxygen hole states that near the edges of valence and conduction band edges within charge states of -1, 0, and +1 (Zn=grey, O=red, spin-up hole state=pink, spin-down hole state=green, and spin-up and spin-down electrons=golden and blue). (f) Schematic diagram of the energy lowering down with the symmetry lowers down from D_{3h} to D_{2h}, and the dirac-cone levels was pinned in the mid-gap of the host monolayer of ZnO within the system of graphene/monolayer ZnO.

References

(1) Özgür, Ü.; Alivov, Y. I.; Liu, C.; Teke, A.; Reshchikov, M. A.; Doğan, S.; Avrutin, V.; Cho, S.-J.; Morkoç, H., *J. Appl. Phys.* **2005,** *98*, 041301.

(2) Zhang, S. B.; Wei, S.-H.; Zunger, A., *J. Appl. Phys.* **1998,** *83*, 3192-3196.

(3) Zhang, S. B.; Wei, S. H.; Zunger, A., *Phys. Rev. B* **2001,** *63*, 075205.

(4) Kobayashi, A.; Sankey, O. F.; Dow, J. D., *Phys. Rev. B* **1983,** *28*, 946-956.

(5) Schoenhalz, A. L.; Arantes, J. T.; Fazzio, A.; Dalpian, G. M., *J. Phys. Chem. C* **2010,** *114*, 18293-18297.

(6) Schoenhalz, A. L.; Dalpian, G. M., *Phys. Chem. Chem. Phys.* **2013,** *15*, 15863-15868.

(7) Zhang, J.; Sun, L.; Liao, C.; Yan, C.-H., **2002,** 262-263.

(8) Zhang, J.; Sun; Yin; Su; Liao; Yan, C.-H., *Chem. Mater.* **2002,** *14*, 4172-4177.

(9) Wu, Z. L.; Merz, J. L.; Werkhoven, C. J.; Fitzpatrick, B. J.; Bhargava, R. N., *Appl. Phys. Lett.* **1982,** *40*, 345-346.

(10) Huang, B., *Physica Status Solidi (b)* **2015,** *252*, 431-441.

(11) Huang, B.; Robertson, J., *Phys. Rev. B* **2012,** *85*, 125305.

(12) Huang, B.; Robertson, J., *J. Non-cryst. Solids.* **2012,** *358*, 2393-2397.

(13) Park, C. H.; Zhang, S. B.; Wei, S.-H., *Phys. Rev. B* **2002,** *66*, 073202.

(14) Li, J.; Wei, S.-H.; Li, S.-S.; Xia, J.-B., *Phys. Rev. B* **2006,** *74*, 081201.

(15) Lyons, J. L.; Janotti, A.; Van de Walle, C. G., *Appl. Phys. Lett.* **2009,** *95*, 252105.

(16) Perdew, J. P.; Burke, K.; Ernzerhof, M., *Phys. Rev. Lett.* **1996,** *77*, 3865-3868.

(17) Vladimir, I. A.; Aryasetiawan, F.; Lichtenstein, A. I., *J. Phys.: Condens. Matter* **1997,** *9*, 767.

(18) Huang, B.; Gillen, R.; Robertson, J., *J. Phys. Chem. C* **2014,** *118*, 24248-24256.

(19) Huang, B., *Philosophical Magazine* **2014,** *94*, 3052-3071.

(20) Huang, B., *Inorg. Chem.* **2015,** *54*, 11423-11440.

(21) Meyer, B., *Phys. Rev. B* **2004,** *69*, 045416.

(22) Anisimov, V. I.; Zaanen, J.; Andersen, O. K., *Phys. Rev. B* **1991,** *44*, 943-954.

(23) Huang, B., *J. Comput. Chem.* **2015,** ***Accepted,*** *DOI: 10.1002/jcc.24272*.

(24) Ma, X.; Wu, Y.; Lv, Y.; Zhu, Y., *J. Phys. Chem. C* **2013,** *117*, 26029-26039.

(25) Lany, S.; Zunger, A., *Phys. Rev. B* **2008,** *78*, 235104.

(26) Oba, F.; Togo, A.; Tanaka, I.; Paier, J.; Kresse, G., *Phys. Rev. B* **2008,** *77*, 245202.

(27) Clark, S. J.; Segall, M. D.; Pickard, C. J.; Hasnip, P. J.; Probert, M. I. J.; Refson, K.; Payne, M. C., *Z. Kristallogr.* **2005,** *220*, 567.

(28) Clark, S. J.; Robertson, J.; Lany, S.; Zunger, A., *Phys. Rev. B* **2010,** *81*, 115311.

(29) Clark, S. J.; Robertson, J., *Physica Status Solidi (b)* **2011,** *248*, 537-546.

(30) Tsukazaki, A.; Ohtomo, A.; Onuma, T.; Ohtani, M.; Makino, T.; Sumiya, M.; Ohtani, K.; Chichibu, S. F.; Fuke, S.; Segawa, Y.; Ohno, H.; Koinuma, H.; Kawasaki, M., *Nat Mater* **2005,** *4*, 42-46.

(31) Pickard, C. J.; Winkler, B.; Chen, R. K.; Payne, M. C.; Lee, M. H.; Lin, J. S.; White, J. A.; Milman, V.; Vanderbilt, D., *Phys. Rev. Lett.* **2000,** *85*, 5122-5125.

(32) Pan, M.; Nause, J.; Rengarajan, V.; Rondon, R.; Park, E. H.; Ferguson, I. T., *J. Electron. Mater.* **2007,** *36*, 457-461.

(33) Liu, W.; Gu, S. L.; Ye, J. D.; Zhu, S. M.; Wu, Y. X.; Shan, Z. P.; Zhang, R.; Zheng, Y. D.; Choy, S. F.; Lo, G. Q.; Sun, X. W., *J. Cryst. Growth* **2008,** *310*, 3448-3452.

(34) Zeuner, A.; Alves, H.; Hofmann, D. M.; Meyer, B. K.; Hoffmann, A.; Haboeck, U.; Strassburg, M.; Dworzak, M., *Physica Status Solidi (b)* **2002,** *234*, R7-R9.
(35) Lany, S.; Zunger, A., *Phys. Rev. B* **2009,** *80*, 085202.
(36) Lany, S.; Zunger, A., *Phys. Rev. B* **2010,** *81*, 205209.
(37) Liu, L.; Xu, J.; Wang, D.; Jiang, M.; Wang, S.; Li, B.; Zhang, Z.; Zhao, D.; Shan, C.-X.; Yao, B.; Shen, D. Z., *Phys. Rev. Lett.* **2012,** *108*, 215501.
(38) Janotti, A.; Van de Walle, C. G., *Phys. Rev. B* **2007,** *76*, 165202.
(39) Oliver, S.; Peter, K.; Chris, G. V. d. W.; Noble, M. J.; Jeff, N.; Gottfried, H. D., *Jpn. J. Appl. Phys.* **2005,** *44*, 7271.
(40) Schmidt, O.; Geis, A.; Kiesel, P.; Van de Walle, C. G.; Johnson, N. M.; Bakin, A.; Waag, A.; Döhler, G. H., *Superlattice. Microst* **2006,** *39*, 8-16.
(41) Dorenbos, P., *J. Electrochem. Soc.* **2005,** *152*, H107-H110.
(42) Hideyuki, M.; Isao, S.; Naoki, O.; Shoichi, S.; Hajime, H.; Junzo, T.; Noboru, I., *Jpn. J. Appl. Phys.* **2003,** *42*, 75.
(43) Yuan, G. D.; Zhang, W. J.; Jie, J. S.; Fan, X.; Zapien, J. A.; Leung, Y. H.; Luo, L. B.; Wang, P. F.; Lee, C. S.; Lee, S. T., *Nano Lett.* **2008,** *8*, 2591-2597.
(44) Yao, Q.; Liu, Y.; Lu, R.; Xiao, C.; Deng, K.; Kan, E., *RSC Adv.* **2014,** *4*, 17478-17482.
(45) Hu, W.; Li, Z.; Yang, J., *J. Chem. Phys.* **2013,** *138*, 124706.
(46) Geng, W.; Zhao, X.; Liu, H.; Yao, X., *J. Phys. Chem. C* **2013,** *117*, 10536-10544.
(47) Geng, W.; Zhao, X.; Zan, W.; Liu, H.; Yao, X., *Phys. Chem. Chem. Phys.* **2014,** *16*, 3542-3548.
(48) Lany, S.; Zunger, A., *Phys. Rev. B* **2010,** *81*, 205209.

For Table of Contents Only

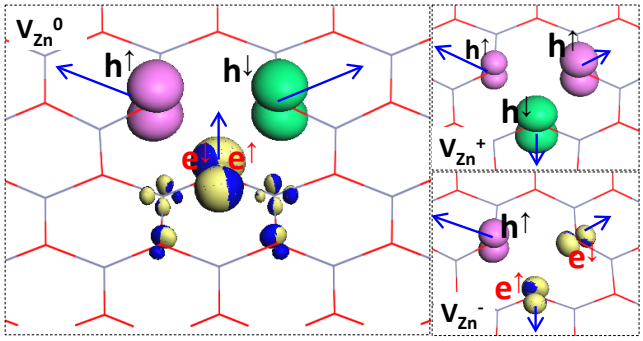

2-D monolayer ZnO (0001) has the localized hole states with the π-like orbital next to the conduction band minimum, and perpendicular to the plane (0001) in real space with p_z-orbital character (with a_1-symmetry). However, the electron acceptor site has similar π-like orbital along the (0001) plane, which is a feature of p_{xy}-orbital. This interesting behavior leads the monolayer ZnO system has an anti-ferromagnetic feature with existence of single neutral V_{Zn} that restricts the Fermi level.